

PAPER

Classification of Prostate Histopathology Images Based on Multifractal Analysis

Chamidu ATUPELAGE^{†a)}, Hiroshi NAGAHASHI^{††}, Masahiro YAMAGUCHI^{†††}, Members, Tokiya ABE^{††††}, Akinori HASHIGUCHI^{††††}, and Michiie SAKAMOTO^{††††}, Nonmembers

SUMMARY Histopathology is a microscopic anatomical study of body tissues and widely used as a cancer diagnosing method. Generally, pathologists examine the structural deviation of cellular and sub-cellular components to diagnose the malignancy of body tissues. These judgments may often subjective to pathologists' skills and personal experiences. However, computational diagnosis tools may circumvent these limitations and improve the reliability of the diagnosis decisions. This paper proposes a prostate image classification method by extracting textural behavior using multifractal analysis. Fractal geometry is used to describe the complexity of self-similar structures as a non-integer exponent called fractal dimension. Natural complex structures (or images) are not self-similar, thus a single exponent (the fractal dimension) may not be adequate to describe the complexity of such structures. Multifractal analysis technique has been introduced to describe the complexity as a spectrum of fractal dimensions. Based on multifractal computation of digital imaging, we obtain two textural feature descriptors; i) local irregularity: α and ii) global regularity: $f(\alpha)$. We exploit these multifractal feature descriptors with a texton dictionary based classification model to discriminate cancer/non-cancer tissues of histopathology images of H&E stained prostate biopsy specimens. Moreover, we examine other three feature descriptors; Gabor filter bank, LM filter bank and Haralick features to benchmark the performance of the proposed method. Experiment results indicated that the performance of the proposed multifractal feature descriptor outperforms the other feature descriptors by achieving over 94% of correct classification accuracy.

key words: histopathology, prostate cancer, fractal geometry, multifractal, feature descriptors, classification

1. Introduction

As reported by Globocan 2008 [1], prostate cancer is the second most frequently diagnosed cancer of men and fifth most common cancer in overall. Histopathological examination is one of the most reliable methods used for diagnosing prostate cancers. In a histopathological examination, pathologists determine the malignancy of body tissues by identifying the structural deviation of cells or sub-cellular components with respect to their healthy stage. However, these judgments may subjective to the pathologists' skills

and experiences, because of the complexity and diversity of histopathology image texture. Figure 1 shows two prostate histopathology images of cancer and non-cancer regions. In the last two decades, medical diagnosis routines have been partially replaced by Computer Aided Diagnosis (CAD) systems [2]. Particularly, the image analysis based CAD systems observe the structural behavior of the texture or cellular/sub-cellular components using mathematical feature descriptors and discriminate the images according to a quantitative scale.

Various texture feature description methods have been proposed to interpret the texture of medical images, e.g., grey-level co-occurrence matrices [3], wavelet transformations [4], filter banks [5]. Adopting fractal and multifractal analysis to describe the texture is a different approach which is recently being used in the medical imagery research [6]. Fractal and multifractal features describe the behavior of texture from self-similarity viewpoint. This approach has been found to be very effective for describing the tumor architecture in histology images [7], [8].

Histopathology texture often exhibits chaotic and irregular patterns and can be categorized statically into broad class of irregular shaped objects. As a consequence, fractal geometry may appropriately describe the irregular texture patterns of histopathology images. The use of fractal geometry for histopathology images can be found in [9]–[11].

This paper proposes a novel textural feature descriptor based on the fractal geometry. Fractal dimension (FD) of an object is a non-integer exponent, which can be used to describe the complexity of self-similar structure. Multifractal analysis is a generalization of fractal analysis, which aims to describe natural structures (or images) as a spec-

Manuscript received March 13, 2012.

[†]The author is with the Department of Computational Intelligence and Systems Science, Tokyo Institute of Technology, Yokohama-shi, 226-8503 Japan.

^{††}The author is with Imaging Science and Engineering Laboratory, Tokyo Institute of Technology, Yokohama-shi, 226-8503 Japan.

^{†††}The author is with Global Scientific Information and Computing Center, Tokyo Institute of Technology, Tokyo, 152-8550 Japan.

^{††††}The authors are with the Department of Pathology, School of Medicine, Keio University, Tokyo, 160-8582 Japan.

a) E-mail: atupelage.c.aa@m.titech.ac.jp

DOI: 10.1587/transinf.E95.D.3037

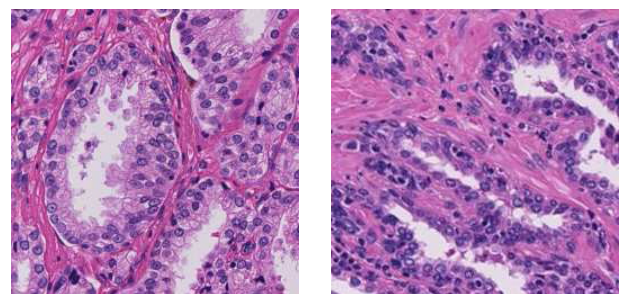


Fig. 1 H&E stained prostate histopathology images of cancer and non-cancer.

trum of fractal dimensions. Based on the multifractal computation of digital images, one may extract two types of textural features, i.e., i) local irregularity: α describes the local behavior of the pixels associated with its neighbors, and ii) global regularity: $f(\alpha)$ describes the distribution of different scales of local irregularities over the entire image. Additionally, multifractal computation is subject to a function called multifractal measure, which defines a scheme to observe the dissimilarity of the pixels in a given region. In this study, we utilize five multifractal measures to derive five-dimensional feature spaces for each α and $f(\alpha)$. The multifractal feature space may extract important textural information, which may not be observable in gray-scale pixel domain. Furthermore, we exploit the proposed feature descriptor with texon dictionary based classification model to classify prostate histopathology images into cancer and non-cancer classes.

In this study, the proposed method was experimentally evaluated as a classification problem. We classified a set of prostate histopathology images into two classes; cancer and non-cancer by using three non-parametric classifiers; Support Vector Machine (SVM), Random Forest and Ada boost. The performance of each classifier was estimated using different metrics; classification accuracy, sensitivity and specificity. Furthermore, we investigated classification performances of other feature extraction methods; Gabor filter bank, LM filters (Leung and Malik) [12] and Haralick features for the same dataset.

The paper is organized as follows; Sect. 2 reviews different feature extraction methods proposed for medical image classification, Sect. 3 describes the theory behinds the fractal and multifractal computations, Sect. 4 illustrates the proposed feature descriptor and the classification model, Sect. 5 gives implementation details of the experiments and analysis of results, and finally Sect. 6 concludes the entire work.

2. Related Work

Based on the feature extraction techniques, histopathology image classification systems can be categorized into three classes; i) Class I extracts the morphological features of cellular or sub-cellular components such as nuclei, lumen and cytoplasm. ii) Class II extracts the textural features by using a feature descriptor such as filter banks, Haralick operator, fractal computation and so on. iii) Class III extracts both morphological and textural features. Each method has different advantages and disadvantages. For an example, performance of class I methods is based on the segmentation accuracy of desired cellular or sub-cellular components. To the contrary, class II methods may overcome that limitation by observing the characteristics of the entire texture. However, they may extract some undesired texture regions such as muscles. This section illustrates different feature extraction methods proposed for medical image classification.

Class III feature extraction algorithm has been proposed for automatic grading of histopathology prostate im-

ages in [13]. They segmented the glandular regions by clustering the feature space derived by wavelet transformation. Both morphological and textural features of glandular regions have used to classify prostate histopathology images into five cancer grades. A tree-structured classification model has used for the classification. For two prostate datasets, the method achieved about 95% and 85% of correct classification rates, respectively.

To identify the malignant tissues of prostate images, a class III feature extraction method has proposed in [14]. This method divided a given region of interest (ROI) of whole slide image (WSI) into 100×100 pixels of sub-regions and each sub-region is classified into three classes; normal, stroma and prostatic carcinoma. They have used Haralick operator [15] to extract textural features and segmentation results of glands to extract morphological features. They evaluated the performance of the system by comparing automated segmented results with conventional pathologist's annotations. As experimental results shown, 79.3% of sub regions of 8 WSIs has been successfully identified.

In [16], a different class III feature extraction method has been proposed to discriminate histopathology prostate images. This method used three textural features; color histogram (16-bins histogram for each color channel of RGB color space), fractal dimension [17] and fractal code [18]. Morphological features of sub-cellular components such as nuclei, cytoplasm, luman were extracted by using a system called MAGIC [19]. They have used Gaussian, k -nearest neighbor and SVM classifiers with sequential forward feature selection algorithm for classifying prostate image dataset. As indicated by the experimental results, this method has classified cancer/non-cancer images with 96.7% of accuracy and high/low grades of cancer images with 81.0% of accuracy.

Fractal geometric computation based class II feature extraction method was proposed in [11] for grading of prostate carcinoma. They used differential box counting (DBC) method [20] and entropy-based fractal dimension computation method to extract the textural features. Both methods involve partitioning the intensity surface into different sizes of grids. They have used four set of different grid sizes with each computation method and obtained eight dimensional feature space. The proposed feature extraction method was evaluated by classifying a set of prostate histopathology images. This method has obtained around 94% of correct classification rate for multi-class classification of four cancer grades.

Another fractal geometric based class II feature extraction method has been proposed to classify digital mammograms [21]. In their method, a given reference image is individually processed by using five image processing operators; smoothing operator toward horizontal and vertical directions, threshold operator for high and low intensities and smoothing operator by averaging four neighboring pixels, respectively and obtained six-images including non-processed one. They compute FD for each image by using differential box counting method and obtained 6-

dimensional feature vector to characterize a given reference image. Authors have obtained area under Receiver Operating Characteristics (ROC) curve as 0.923 for two class classification for online mammogram database from Mammographic Image Analysis Society (MIAS).

This paper propose a class II feature extraction method to classify prostate images into cancer and non-cancer classes. Textural features are extracted using multifractal computation with five multifractal measures. As a consequence, five dimensional feature space is obtained to describe the texture. This multifractal feature descriptor is employed into texton based classification model to distinguish cancer and non-cancer tissues of prostate histopathology images of H&E stained biopsy specimens. As far as we know, there have not been proposed any textural feature descriptors that are coherent to our method.

3. Fractal Fundamentals

Mandelbrot proposed a new geometrical model to describe irregular shape objects, later known to be “fractal geometry” [22]. Fractal geometry is based on the idea of self-similar forms. To be self-similar, a shape must be able to be divided into parts, which are more or less similar to the whole. Self-similarity occurs over an infinite range of scales for pure mathematical structures such as Koch’s curve, Cantor set and Sierpinski triangle. However, self-similarity of natural structures is bounded in finite range of scales [23].

In 1984, Pentland showed that intensity surfaces of natural images are partially isotropic fractals. This idea was evolved to describe the roughness of the intensity surfaces of digital images and successfully applied in many digital image processing and medical imaging applications [7], [8], [11], [21], [24]–[26].

3.1 Fractal and Multifractal

Fractal dimension (FD) of an object is a non-integer exponent, which strictly exceed the topological dimension and computed by using the *Hausdorff-Besicovitch* definition [23].

Let Θ be a bounded subset of \mathbb{R}^n and $N_\varepsilon(\Theta)$ be the minimum number of balls of radius ε required to cover Θ . When ε tends to 0^+ , the limiting values of $N_\varepsilon(\Theta)$ follows the power law $N_\varepsilon(\Theta) \sim \varepsilon^{-d_H}$, where d_H is a constant, i.e., the FD of Θ .

$$d_H(\Theta) = - \lim_{\varepsilon \rightarrow 0^+} \frac{\log(N_\varepsilon(\Theta))}{\log(\varepsilon)} \quad (1)$$

Deterministic structures (mathematically generated by applying the same rule recursively) can be characterized by the same fractal dimension in all scales. In contrast, natural structures are non-deterministic, thus, a single FD may not be adequate to characterize such structures. Multifractal analysis is a generalization of fractal geometrical analysis, which characterizes irregular natural structures as a spectrum of FDs, i.e., multifractal spectrum. Multifractal com-

putation is carried out in two consecutive steps.

At the first step, one may find the local irregularity of a function μ called “multifractal measure” at a point x of set S , as a non-integer exponent, which is described by an Hölder Exponent $h_\mu(x)$,

$$h_\mu(x) = \lim_{r \rightarrow 0^+} \frac{\log(\mu(B(x, \varepsilon)))}{\log(\varepsilon)}, \quad (2)$$

where $B(x, \varepsilon)$ stands for the closed ball of radius r centered at x .

Multifractal analysis of set S consists of computing FD of different size of level sets of h_μ ,

$$E_h^\mu = \{x|h_\mu(x) = h\}. \quad (3)$$

where, E_h^μ is a set of points, whose exponents are equal to h .

At the second step, one may estimate FD of E_h^μ for different h of h_μ and form a spectrum d_μ , i.e., multifractal spectrum of S [27],

$$h \mapsto d_\mu(h) = \dim(E_h^\mu), \quad (4)$$

where, $\dim(E_h^\mu)$ stands for the FD of the set E_h^μ .

3.2 Multifractal Analysis on Digital Image

A digital gray scale image can be described by two-dimensional real and non-negative function of gray $g(x, y)$, where x and y are discrete spatial coordinates of the image. Therefore, it is necessary to modify the definitions given in Sect. 3.1 to be appropriate for digital images. It turns out that the limiting value of ε becomes 1^+ and B becomes a square of side length ε in Eq. (2).

$$h_\mu(x, y) = \lim_{\varepsilon \rightarrow 1^+} \frac{\log(\mu(W_\varepsilon(x, y)))}{\log(\varepsilon)}, \quad (5)$$

where $W_\varepsilon(x, y)$ stands for the window of side length ε centered at (x, y) .

In the computation, one may plot $\log(\mu(W_\varepsilon(x, y)))$ against to $\log(\varepsilon)$ for $\varepsilon = 2i + 1, i = 1, 2, \dots$ and estimate the gradient of linear regression line as the local irregularity at point (x, y) . Similarly, by computing $h_\mu(x, y)$ for every pixel of the reference image, we can derive a matrix of same dimension, which is α feature matrix (or α image).

Subsequently, we quantize the entire range of α (from minimum to maximum) into R discrete sub-ranges. Let α_r be all α values quantized into r^{th} sub-range. α_r may be formed a binary value matrix I_{α_r} , which has the same dimension of α matrix.

$$I_{\alpha_r}(x, y) = \begin{cases} 1, & \alpha_{rMin} \leq \alpha(x, y) < \alpha_{rMax} \\ 0, & otherwise \end{cases} \quad (6)$$

where, α_{rMin} and α_{rMax} stand for lower and upper limit of r^{th} sub-range, $\alpha(x, y)$ be the value at point (x, y) in α matrix.

Subsequently, it is required to compute FD of each I_{α_r} , according to Hausdorff-Besicovitch definition. There

are numerous Hausdorff-Besicovitch dimension computation algorithms and each method has its own theoretic basis to estimate the parameter N in Eq. (1) [6]. Among them, box-counting algorithm is one of the popular FD estimation methods, because of its efficiency, accuracy and easy implementation [28].

To estimate the FD of a binary image I , one may cover the entire image using a grid of side length ε' and count the number of non-empty boxes $N_{\varepsilon'}(I)$. For digital imaging, ε' tends to 1^+ . The FD of I is the box-counting dimension d_B .

$$d_B(I) = \lim_{\varepsilon' \rightarrow 1^+} \frac{\log(N_{\varepsilon'}(I))}{\log(\varepsilon'^{-1})} \quad (7)$$

Accordingly, one may plot $\log(N_{\varepsilon'}(I))$ against $\log(\varepsilon'^{-1})$ for $\varepsilon' = 1, 2, \dots$, and estimate the gradient of linear regression line as the FD of I . In this manner, we obtain FD for each I_{α_r} and form a multifractal spectrum, which is referred as $f(\alpha)$. Additionally, for each element in the α matrix, we can find a corresponding $f(\alpha)$ values, which leads to a matrix called $f(\alpha)$ (or $f(\alpha)$ image) of the same dimension to the α matrix.

As a consequence, multifractal computation can be utilized to obtain two kinds of textural features; local irregularity: α and global regularity: $f(\alpha)$, respectively.

4. Methodology

The proposed method utilizes the multifractal analysis to describe the texture of histopathology images in a high dimensional feature space. This section illustrates the proposed feature extraction method and its utilization for a texture classification problem.

4.1 Multifractal Feature Descriptor

The textural features presented in α and $f(\alpha)$ are subjective to some multifractal measure μ (refer Eq. (5)). It turns out that different types of multifractal features can be obtained by appropriately choosing different multifractal measures. In our investigation, we empirically selected five multifractal measures to describe the texture. As a consequence, we obtained five dimensional feature spaces for each α and $f(\alpha)$.

Three multifractal measures; Maximum: μ_{Max} , Minimum: μ_{Min} and Summation: μ_{Sum} , were selected from [29] and definitions are provided in Eqs. (8a), (8b) and (8c), respectively. We obtain normalized difference in between maximum and minimum intensities of a particular window as a multifractal measure; Ndiff: μ_{Ndiff} as shown in Eq. (8d) [30]. These four measures observe the disparity of the gray intensities from four different viewpoints. In addition, gradient operator is widely used to extract the edge information of complex texture. Therefore, we select another measure; Gradient: μ_{Grad} proposed in [24] and its definition is given in Eq. (8e), which allow us to analyze the texture through its gradient behavior.

$$\mu_{Max}(m, n) = \max_{(k,l) \in \Omega} g(k, l) \quad (8a)$$

$$\mu_{Min}(m, n) = \min_{(k,l) \in \Omega^*} g(k, l) \quad (8b)$$

$$\mu_{Sum}(m, n) = \sum_{(k,l) \in \Omega} g(k, l) \quad (8c)$$

$$\mu_{Ndiff}(m, n) = \left(\max_{(k,l) \in \Omega} g(k, l) - \min_{(k,l) \in \Omega^*} g(k, l) \right) / \varepsilon \quad (8d)$$

$$\mu_{Grad}(m, n) = \left(\|G_m\|^2 + \|G_n\|^2 \right)^{1/2} \quad (8e)$$

where, $\mu_{(\cdot)}(m, n)$ stands for the amount of measure at point (m, n) . Ω is the window of side length ε centered at point (m, n) . Ω^* represents the non-zero pixels of the Ω . $g(k, l)$ is the gray intensity at point (k, l) . G_m and G_n stand for gradient vectors at point (m, n) towards horizontal and vertical directions, respectively.

Furthermore, Fig. 2 shows the appearance of α and $f(\alpha)$ features obtained for the image in Fig. 1 (a), corresponding to each multifractal measure described in Eqs. (8a)–(8e). For finer visualization, we have normalized each image into gray-scale [0, 255].

4.2 Classification Model

In this study, we employed the proposed multifractal feature descriptor with a texton dictionary based classification model to distinguish cancer and non-cancer tissues of prostate histopathology images. Texton dictionary is a collection of distinct texture primitives [31] that can be used to dictate a given texture [32]. When the texture is described in high dimensional feature space, the texton becomes a vector, which has the same dimension to the feature space, the dictionary is a collection of vectors. In addition, the texton dictionary should have an adequate number of distinct textons to describe a given image [12], [33]. More precisely, to obtain high accuracy in the classifier, the texton dictionary should have all possible types of distinct textons of the measured domain[†]. One may construct the texton dictionary by clustering the entire feature-pool^{††}, which is derived by using every possible image in the measured domain, and subsequently, find the centroid of each cluster as the element of the dictionary.

In texton dictionary based classification model, the dictionary is used to label all the pixels of an image, which is called texton labeling. One may find the closest texton for each feature vector of the reference image and label each pixel by the corresponding texton's index. The closest texton is the one, which has minimum Euclidean distance to the given feature vector. Subsequently, one computes a histogram for the labeled image, where each bin represents

[†]Generally, computing a universal texton dictionary is impractical. Therefore, one may derive a texton dictionary for a particular kind of images, i.e., measured domain, e.g., H&E stained prostate histopathology images captured in 20x magnification.

^{††}Feature pool is a collection of feature vectors obtain from feature spaces of a set of images.

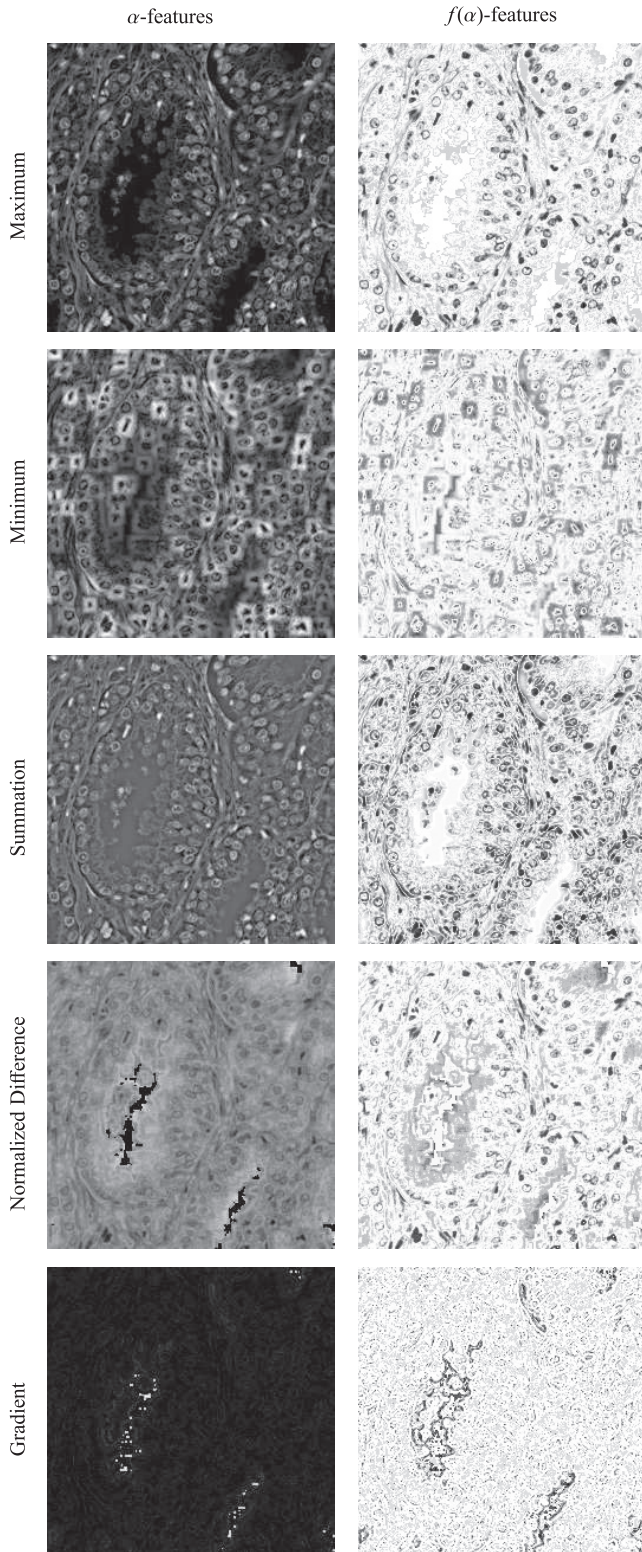


Fig. 2 Appearance of different multifractal features of the reference image Fig. 1 (a). Left and right columns present the α and $f(\alpha)$ features respectively. From top to bottom, each row represents multifractal measures; Maximum, Minimum, Summation, Normalized Difference and Gradient, respectively. All images have been normalized to grey scale: [0~255] for clear visualization.

the texton’s index (label) and its value indicates the number of occurrences of that label in the entire image. This histogram may be called texture signature of the reference image, because it comprises all characteristics of the image with respect to the utilized feature descriptor.

Subsequently, these texture signatures (feature vectors) are classified by using an appropriate supervised learning classifier. There are two types of supervised learning classifiers; parametric and non-parametric. Parametric classifiers assume that functional forms of the class-conditional distributions are known and non-parametric classifiers make minimal assumptions of class-conditional distributions. The choice of the classifier depends on the sample size and prior knowledge about the class conditional distributions.

5. Experimental Results and Analysis

We examined the performance of the proposed multifractal feature descriptor together with texton dictionary based classification model by classifying a set of prostate histopathology image dataset. This section illustrates; data acquisition, computational parameters of multifractal and other comparative feature descriptors, performance evaluation metrics and the results.

5.1 Data Acquisition

We obtained a sample dataset of H&E (hematoxylin and eosin) stained prostate biopsy specimens of 11 cases. Each sample specimen is scanned as a Whole Slide Image (WSI) of 20x magnification using scanner called Nano-Zoomer. Each WSI can be visualized in eight resolutions such as 1.25x, 2.5x, 5x, 10x, 20x, 40x, 63x, and 100x through a digital slider called NDPViewer. Both Nano-Zoomer and NDPViewer are products of Hamamatsu Photonic K. K.. The approximate size of the WSI at 20x resolution is 33600 × 21000 pixels. The cancer regions of each WSI have been annotated by several experienced pathologists.

The appearances of the components of prostate tissues such as nuclei, cytoplasm, lumen, cell membrane, etc., are slightly varied with the resolution of the WSI. Therefore, pathologists use several resolutions in the digital slider for diagnosing malignant tissues. Moreover, they often use the original resolution (e.g., 20x) or its closer resolutions in the digital slider, because more higher or lower resolution (with respect to the original resolution) images may comprise some visual artifacts. In our experiment, we set up 3 categories of image datasets corresponding to 10x, 20x and 40x resolutions. For each category, by using 11 WSIs, we select 600 sample patches of size 256 × 256 pixels in equal amounts for each cancer and non-cancer regions.

5.2 Multifractal Features Extraction

In our experiment, we compute the α features according to the definition given in Eq. (5) by setting ε as 1, 3, 5, 7, 9, 11, 13. Subsequently, to compute $f(\alpha)$ features, we quan-

tized α range into 70 discrete sub-ranges and estimated the FD for each sub-range for $\epsilon' = 1, 2, 4, 6, 8, 10, 12, 14, 16$ as defined in Eq. (7). By repeating this procedure for each multifractal measures described in Eqs. (8a)–(8e), we obtained 5-dimensional α and $f(\alpha)$ feature spaces for each image in the datasets.

5.3 Feature Descriptors for Comparison

The performance of the proposed multifractal feature descriptor is compared with three other widely used feature descriptors; Gabor filters [34], LM-filters [12] and Haralick features [15].

Gabor filter bank method is a promising textural feature extraction technique among existing multi-channel filtering approaches. Gabor filter is generated by modulating an oriented sinusoidal plane of particular frequency with a Gaussian envelope. The design of Gabor filter bank is arbitrary or application oriented. Basically, one may generate the filter bank by utilizing two parameters; spatial frequency: $\lambda = 0.25 - 2^{(i-0.5)/N}$, where $N =$ image width, and orientation: θ [34]. Our experimental Gabor filter bank was constructed for $i = 1, 2, 3, 4, 5$ and $\theta = 0^\circ, 45^\circ, 90^\circ, 135^\circ$. As a consequence, we obtained 20-dimensional feature space to describe the texture.

LM-filter bank has been successfully applied to recognize the texture of materials made up of both reflectance and surface normal variations. The LM filter bank consists of 48 filters; first and second derivative of Gaussian filters of 6 orientations and 3 scales making total of 36 filters, 8 Laplacian of Gaussian filters, and 4 Gaussian filters. LM-filter bank allows us to describe the texture in 48-dimension of feature space.

On the other hand, Haralick texture features have been used in many image understanding applications including medical and geographical imaging. The calculation of Haralick features are carried out in two consecutive stages; i) construction of the co-occurrence matrix and, ii) calculation of 13 texture features based on the co-occurrence matrix. Two parameters were concerned for constructing co-occurrence matrix such as scalar distance: s and orientation: θ . In this experiment, we used $s = 2$ and $\theta = 0^\circ, 45^\circ, 90^\circ, 135^\circ$ to compute the co-occurrence matrix. We empirically decided the value for s by obtaining maximum correct classification rate for 20x resolution image dataset with SVM. Subsequently, we computed the features; Angular Second Moment, Contrast, Correlation, Sum of Squares: Variation, Inverse Difference Moment, Sum Average, Sum Variance, Sum Entropy, Entropy, Difference Variance, Difference Entropy, Information Measure of Correlation 1 and Correlation 2, for each co-occurrence matrix. As a consequence, we obtained 52-dimensional feature space to characterize a given image.

5.4 Classification

We utilized k -means clustering with $k = 300$ to construct

texton dictionaries for feature descriptors; α , $f(\alpha)$, Gabor and LM. We empirically decided that 300 textons are adequate to obtain optimal correct classification rate. As a consequence, α , $f(\alpha)$, Gabor and LM feature sets use 300 dimension of feature vector (histogram of 300 bins) to characterize the texture of a given image. Haralick feature descriptor uses 52-dimension feature vector. Subsequently, we utilized these feature vectors with three supervised learning non-parametric classifiers; SVM [35], Ada Boosting [36] and Random Forest [37] to perform two-class classification; cancer and non-cancer. As the implementations of the classifiers we used MatLab SVM toolbox [38], GML AdaBoost Matlab Toolbox [39] and Randomforest-Matlab [40].

5.5 Performance Estimation

Typical supervised learning based classification systems have two stages; i) learning: the classifier learns the system parameters, ii) testing: the classifier makes prediction to evaluate the performance of the system. For a small sample set, k -fold cross validation is one of the popular strategy used to reduce bias of the classifier in machine learning and testing [41]. In our experiment, 10-fold cross validation is performed, namely, in every iteration 540 samples were elected for learning and 60 samples were used for testing.

We used several statistical error estimation metrics to compare the performance of feature descriptors. The metric of correct classification rate CCR is estimated as $CCR = n_c/n$, where n_c denotes the number of correctly classified samples and n is the total number of samples used for testing. Additionally, the predictions of a binary class classification diagnostic system derives a confusion matrix of four possible parameters; i) True Positive (TP), ii) True Negative (TN), iii) False Positive (FP) and iv) False Negative (FN). We computed two statistical measures; *Sensitivity* and *Specificity* from the confusion matrix as $sensitivity = TP/(TP + FN)$ and $specificity = TN/(FP + TN)$. More precisely, sensitivity measures the proportion of correctly identified actual positives and specificity measures the proportion of correctly identified actual negatives. The diagnostic systems aim to achieve 100% for both sensitivity and specificity. The averages of CCR, sensitivity and specificity in each iteration of the cross-validation were taken to examine the performance of the classification.

5.6 Results and Discussion

We examined the classification performance through CCR, sensitivity and specificity as shown in Tables 1 and 2. Table 1 has categorized the results as classifier, resolution (magnification scale) of the dataset and feature descriptor. Table 2 presents the average performance of each feature descriptor of all three resolutions of image datasets. We have used the format $x \pm y$ to present the CCR, where x and y are sample mean and standard error for 95% confidence interval respectively.

It is apparent from Table 1 that for every resolution

Table 1 Classification results for SVM, RandomForest and AdaBoosting classifier.

	Resolution	Feature	CCR (%)	Sensitivity (%) / Specificity (%)
SVM	10x	α	95.80±3.66	91.00 / 90.50
		$f(\alpha)$	95.20±4.29	92.00 / 91.50
		Gabor	84.00±4.39	88.67 / 79.33
		LM	82.17±3.85	86.67 / 77.67
		Haralick	83.00±7.53	88.33 / 77.67
	20x	α	94.90±3.69	90.20 / 90.00
		$f(\alpha)$	95.18±4.12	92.50 / 91.00
		Gabor	80.00±5.09	79.00 / 76.00
		LM	81.50±7.00	86.67 / 86.33
		Haralick	84.33±4.86	88.33 / 80.33
	40x	α	93.20±4.22	92.50 / 89.50
		$f(\alpha)$	93.40±5.88	91.50 / 90.50
		Gabor	81.73±6.11	74.00 / 69.67
		LM	81.83±5.90	75.33 / 68.33
		Haralick	83.67±4.98	86.67 / 74.67
RandomForest	10x	α	92.50±5.50	94.00 / 91.00
		$f(\alpha)$	91.25±5.83	90.50 / 89.80
		Gabor	83.00±5.82	81.00 / 85.00
		LM	82.67±4.79	81.00 / 84.33
		Haralick	85.83±3.26	87.00 / 84.67
	20x	α	90.80±4.44	91.00 / 81.00
		$f(\alpha)$	91.50±4.97	89.50 / 81.50
		Gabor	75.17±3.37	73.67 / 76.67
		LM	78.50±4.34	75.33 / 81.67
		Haralick	82.67±5.16	85.00 / 80.33
	40x	α	92.25±4.63	92.50 / 89.00
		$f(\alpha)$	92.75±7.46	88.00 / 87.50
		Gabor	79.67±4.96	74.00 / 85.33
		LM	82.17±4.16	77.67 / 86.67
		Haralick	84.17±2.97	85.67 / 82.67
AdaBoost	10x	α	91.50±10.01	92.00 / 81.80
		$f(\alpha)$	87.75±5.83	82.00 / 79.50
		Gabor	81.50±5.58	83.67 / 79.33
		LM	78.33±7.16	77.33 / 89.33
		Haralick	83.33±4.37	85.67 / 81.00
	20x	α	89.75±6.40	86.00 / 83.50
		$f(\alpha)$	89.75±12.10	72.50 / 71.70
		Gabor	48.67±8.53	76.00 / 21.33
		LM	67.50±7.42	75.00 / 40.00
		Haralick	81.33±6.56	83.67 / 79.00
	40x	α	91.75±9.81	76.00 / 77.60
		$f(\alpha)$	91.00±9.22	88.00 / 64.00
		Gabor	74.50±7.50	70.00 / 69.00
		LM	71.00±9.53	85.00 / 67.00
		Haralick	80.17±6.40	82.67 / 77.67

of image dataset, multifractal features have obtained significant performance for each quality measure compared to the other feature descriptors. Table 2 also concludes that α and $f(\alpha)$ features outperformed other features descriptors irrespective to the magnification of the images. Particularly, Table 2 showed that α and $f(\alpha)$ features have obtained 94.63% and 94.59% of CCR, 91.23% and 92.00% of sensitivity, 90.00% and 91.00 of specificity, respectively with SVM classifier. As a overall summary, both α and $f(\alpha)$ features have obtained over 94% of CCR and over 90% of sensitivity and specificity. It turns out that fractal geometry appropriately describes the complex texture patterns in

Table 2 Average classification performance of each feature.

Feature	Classifier	CCR (%)	Sensitivity (%) / Specificity (%)
α	SVM	94.63±3.86	91.23 / 90.00
	RandomForest	91.85±4.86	92.50 / 87.00
	AdaBoost	91.00±8.74	84.67 / 80.97
$f(\alpha)$	SVM	94.59±4.76	92.00 / 91.00
	RandomForest	91.83±6.09	89.33 / 86.27
	AdaBoost	89.50±9.05	80.83 / 71.73
Gabor	SVM	81.91±5.20	80.56 / 75.00
	RandomForest	79.28±4.72	76.22 / 82.33
	AdaBoost	68.22±7.20	76.56 / 56.55
LM	SVM	81.83±5.58	82.89 / 77.44
	RandomForest	81.11±4.43	78.00 / 84.22
	AdaBoost	72.28±8.04	79.11 / 65.44
Haralick	SVM	83.67±5.79	87.78 / 77.56
	RandomForest	84.22±3.80	85.89 / 82.56
	AdaBoost	81.61±5.78	84.00 / 79.22

prostate histopathology images.

We note here that, feature descriptors α , $f(\alpha)$, Gabor and LM have used 300 dimension of feature vectors; to the contrary, Haralick features consisted of 52 dimension of feature vectors. Even though, higher dimension of feature vectors increase the computational cost of the classifier, higher accuracy is anticipated in medical diagnosis systems.

6. Conclusion

Typical histopathological judgments may be subjective and often lead to have considerable variation. To circumvent this issue and improve the reliability of cancer diagnosis, it is important to develop computational tools for classifying histopathologic images that operate on quantitative measures. This paper proposed a new feature descriptor to characterize the texture based on fractal geometry. By using five multifractal measures, we computed two types of multifractal feature descriptions; α and $f(\alpha)$, which provide local irregularity and global regularity information of the texture, respectively. We employed the proposed feature extraction method with texton dictionary based classification model to discriminate a set of images of H&E stained prostate biopsy specimens into cancer and non-cancer classes. Three types of supervised learning classifiers were used, SVM, Random Forest and Ada boost. The performance of each classifier was estimated through three statistical measures; correct classification rate, sensitivity and specificity. Furthermore, the merit of the proposed method was examined by comparing the performance of the proposed method with three textural feature descriptors; Gabor, LM and Haralick. Experimental results indicated that the proposed feature descriptor outperformed the other feature descriptors.

Furthermore, the proposed feature descriptor is independent of the computation of morphological characteristics of tissue level component such as nuclei. Instead, it observes the entire textural information. Therefore, the proposed feature descriptor may be useful for discriminating cancerous

tissues or their grades of other body organs.

Acknowledgment

This research is supported by New Energy and Industrial Technology Development Organization (NEDO) in Japan under the research and development project of Pathological Image Recognition.

References

- [1] J. Ferlay, H. Shin, F. Bray, D. Forman, C. Mathers, and D. Parkin, "Estimates of worldwide burden of cancer in 2008: GLOBOCAN 2008," *International Journal of Cancer*, vol.127, no.12, pp.2893–2917, 2010.
- [2] G. Díaz and E. Romero, "Micro-structural tissue analysis for automatic histopathological image annotation," *Microscopy Research and Technique*, vol.75, pp.343–358, 2011.
- [3] M. Tahir, A. Bouridane, and F. Kurugollu, "An FPGA based coprocessor for GLCM and Haralick texture features and their application in prostate cancer classification," *Analog Integr. Circuits Signal Process.*, vol.43, no.2, pp.205–215, 2005.
- [4] R. Ferrari, R. Rangayyan, J. Desautels, and A. Frere, "Analysis of asymmetry in mammograms via directional filtering with Gabor wavelets," *IEEE Trans. Med. Imaging*, vol.20, no.9, pp.953–964, 2001.
- [5] J. Soares, J. Leandro, R. Cesar, H. Jelinek, and M. Cree, "Retinal vessel segmentation using the 2-D Gabor wavelet and supervised classification," *IEEE Trans. Med. Imaging*, vol.25, no.9, pp.1214–1222, 2006.
- [6] R. Lopes and N. Betrouni, "Fractal and multifractal analysis: A review," *Medical Image Analysis*, vol.13, no.4, pp.634–649, 2009.
- [7] B. Chaudhuri and N. Sarkar, "Texture segmentation using fractal dimension," *IEEE Trans. Pattern Anal. Mach. Intell.*, vol.17, no.1, pp.72–77, 1995.
- [8] J. Baish and R. Jain, "Fractals and cancer," *Cancer Research*, vol.60, no.14, pp.36–83, 2000.
- [9] T. Li, S. Wang, and N. Zhao, "Fractal research of pathological tissue images," *Computerized Medical Imaging and Graphics*, vol.31, no.8, pp.665–671, 2007.
- [10] A. Hemsley and R. Mukundan, "Multifractal measures for tissue image classification and retrieval," 11th IEEE International Symposium on Multimedia, ISM'09, pp.618–623, 2009.
- [11] P. Huang and C. Lee, "Automatic classification for pathological prostate images based on fractal analysis," *IEEE Trans. Med. Imaging*, vol.28, no.7, pp.1037–1050, 2009.
- [12] T. Leung and J. Malik, "Representing and recognizing the visual appearance of materials using three-dimensional textons," *Int. J. Comput. Vis.*, vol.43, no.1, pp.29–44, 2001.
- [13] R. Farjam, H. Soltanian-Zadeh, R. Zoroofi, and K. Jafari-Khouzani, "Tree-structured grading of pathological images of prostate," *Proc. SPIE*, p.840, 2005.
- [14] J. Diamond, N. Anderson, P. Bartels, R. Montironi, and P. Hamilton, "The use of morphological characteristics and texture analysis in the identification of tissue composition in prostatic neoplasia," *Human Pathology*, vol.35, no.9, pp.1121–1131, 2004.
- [15] R. Haralick, K. Shanmugam, and I. Dinstein, "Textural features for image classification," *IEEE Trans. Syst. Man Cybern.*, vol.SMC-3, no.6, pp.610–621, 1973.
- [16] A. Tabesh, M. Teverovskiy, H. Pang, V. Kumar, D. Verbel, A. Kotsianti, and O. Saidi, "Multifeature prostate cancer diagnosis and Gleason grading of histological images," *IEEE Trans. Med. Imaging*, vol.26, no.10, pp.1366–1378, 2007.
- [17] A. Jacquin, "Fractal image coding: A review," *Proc. IEEE*, vol.81, no.10, pp.1451–1465, 1993.
- [18] B. Schouten and P. de Zeeuw, "Feature extraction using fractal codes," *Visual Information and Information Systems*, pp.658–658, 1999.
- [19] C. Cordon-Cardo, A. Kotsianti, D. Verbel, M. Teverovskiy, P. Capodiecici, S. Hamann, Y. Jeffers, M. Clayton, F. Elkhettabi, F. Khan, "Improved prediction of prostate cancer recurrence through systems pathology," *J. Clinical Investigation*, vol.117, no.7, pp.1876–1883, 2007.
- [20] A. Pentland, "Fractal-based description of natural scenes," *IEEE Trans. Pattern Anal. Mach. Intell.*, vol.PAMI-6, no.6, pp.661–674, 1984.
- [21] D. Sankar and T. Thomas, "Fractal features based on differential box counting method for the categorization of digital mammograms," *International Journal of Computer Information Systems and Industrial Management Applications (IJCSIM)*, vol.2, pp.11–19, 2010.
- [22] B. Mandelbrot, "How long is the coast of Britain? Statistical self-similarity and fractional dimension," *Science*, vol.156, no.3775, p.636, 1967.
- [23] B. Mandelbrot, *The fractal geometry of nature*, WH freeman, 1983.
- [24] A. Turiel and N. Parga, "The multifractal structure of contrast changes in natural images: From sharp edges to textures," *Neural Comput.*, vol.12, no.4, pp.763–793, 2000.
- [25] Y. Xia, D. Feng, and R. Zhao, "Morphology-based multifractal estimation for texture segmentation," *IEEE Trans. Image Process.*, vol.15, no.3, pp.614–623, 2006.
- [26] T. Stojić, I. Reljin, and B. Reljin, "Adaptation of multifractal analysis to segmentation of microcalcifications in digital mammograms," *Physica A*, vol.367, pp.494–508, 2006.
- [27] J. Barral and S. Seuret, "Combining multifractal additive and multiplicative chaos," *Communications in Mathematical Physics*, vol.257, no.2, pp.473–497, 2005.
- [28] D. Russell, J. Hanson, and E. Ott, "Dimension of strange attractors," *Phys. Rev. Lett.*, vol.45, no.14, pp.1175–1178, 1980.
- [29] J.L. Vêhel, P. Mignot, et al., "Multifractal segmentation of images," *Fractals*, vol.2, no.3, pp.371–378, 1994.
- [30] A. Górski, "Pseudofractals and the box counting algorithm," *J. Phys. A, Math. Gen.*, vol.34, p.7933, 2001.
- [31] B. Julesz, "Textons, the elements of texture perception, and their interactions," *Nature*, vol.290, pp.91–97, 1981.
- [32] D. Charalampidis, "Texture synthesis: Textons revisited," *IEEE Trans. Image Process.*, vol.15, no.3, pp.777–787, 2006.
- [33] O. Cula and K. Dana, "3D texture recognition using bidirectional feature histograms," *Int. J. Comput. Vis.*, vol.59, no.1, pp.33–60, 2004.
- [34] F. Bianconi and A. Fernández, "Evaluation of the effects of Gabor filter parameters on texture classification," *Pattern Recognit.*, vol.40, no.12, pp.3325–3335, 2007.
- [35] C. Cortes and V. Vapnik, "Support-vector networks," *Mach. Learn.*, vol.20, no.3, pp.273–297, 1995.
- [36] I. Fasel, B. Fortenberry, and J. Movellan, "GBoost: A generative framework for boosting with applications to realtime eye coding," *Computer Vision and Image Understanding*, vol.98, no.1, pp.182–210, 2005.
- [37] L. Breiman, "Random forests," *Mach. Learn.*, vol.45, no.1, pp.5–32, 2001.
- [38] S. Gunn, *MatLab SVM toolbox*, 2001.
- [39] A. Vezhnevets, *GML AdaBoost Matlab Toolbox*, 2008.
- [40] A. Jaiantilal, *Randomforest-Matlab*, 2010.
- [41] K. Fukunaga, *Introduction to statistical pattern recognition*, Academic Press, 1990.



Chamidu Atupelage received B.Sc. from University of Colombo, Sri Lanka in 2004 and M.Eng. from Hiroshima University, Japan in 2009. At present, he is a Ph.D. candidate in Department of Computational Intelligence and Systems Science, Tokyo Institute of Technology. His research interest includes pattern recognition, image processing, medical image analysis in color and multispectral domains.



Akinori Hashiguchi received M.D. and Ph.D. degree from the School of Medicine, Keio University, Tokyo, Japan, in 1995 and 2011. He has worked as an instructor at the Department of Pathology, Keio University, since 1995 and is now engaged in research on digital pathology and pathology informatics.



Hiroshi Nagahashi received his B.S. and Dr.Eng. degrees from Tokyo Institute of Technology in 1975 and 1980, respectively. Since 1990, he has been with Imaging Science and Engineering Laboratory, Tokyo Institute of Technology, where he is currently a professor. His research interests include pattern recognition, computer graphics, image processing, computer vision. Dr. Nagahashi is a member of IEEE Pattern Analysis and Machine Intelligence Society, the Institute of Electrical Engineers of Japan, the

Information Processing Society of Japan.



Michiie Sakamoto received a Ph.D. degree from Keio University School of Medicine in 1991. He was appointed as a research member in Pathology Division, National Cancer Center Research Institute in Tokyo in 1989, and nominated as a chief in the division in 1999. He is currently a Professor at the Department of Pathology, Keio University School of Medicine since 2002. He is an Editor-in-chief of Pathology International, an Associate Editor of Cancer Science and Hepatology Research, and Editorial Board of many kinds of international journals. His research interest is molecular Pathology of Cancer: multistep-carcinogenesis, early cancer, invasion and metastasis and Pathology Informatics.

His research interest is molecular Pathology of Cancer: multistep-carcinogenesis, early cancer, invasion and metastasis and Pathology Informatics.



Masahiro Yamaguchi received B.S., M.Eng., and Ph.D. from Tokyo Institute of Technology in 1987, 1989, and 1994, respectively. He is a professor in Global Scientific Information and Computing Center, Tokyo Institute of Technology since 2011. After he worked as a faculty research associate since 1989, he had been an associate professor in Imaging Science and Engineering Laboratory, Tokyo Institute of Technology. From 1999 to 2006, he had been concurrently a project sub-leader in Akasaka

Natural Vision Research Center, Telecommunication Advancement Organization (TAO, currently NICT), Japan. He has been working on the color and multispectral imaging, holography, medical image processing, and the application of information security technology.



Tokiya Abe received the Ph.D. degree in 2005 from Tokyo Institute of Technology, Yokohama Japan. He worked as postdoctoral researcher at Imaging Science and Engineering Laboratory in Tokyo Institute of Technology from 2005 to 2007. He joined Research Center for Frontier Medical Engineering, Chiba University. From 2008 to 2009, he worked as postdoctoral researcher at Department of pathology in Massachusetts General Hospital. He is currently a projected research associate at the Department of Pathology, Keio University School of Medicine since 2010. His research interest is multi-spectral and histopathological image processing.

His research interest is multi-spectral and histopathological image processing.